



Iterative reconstruction with multifrequency signal recognition technology to improve low-contrast detectability: A phantom study

Acta Radiologica Open
11(6) 1–8
© The Author(s) 2022
Article reuse guidelines:
sagepub.com/journals-permissions
DOI: 10.1177/20584601221109919
journals.sagepub.com/home/arr


Yoshinori Funama¹ , Takashi Shirasaka^{2,3}, Taiga Goto⁴, Yuko Aoki⁴, Kana Tanaka⁴ and Ryo Yoshida⁴

Abstract

Background: Brain CT needs more attention to improve the extremely low image contrast and image texture.

Purpose: To evaluate the performance of iterative progressive reconstruction with visual modeling (IPV) for the improvement of low-contrast detectability (IPV-LCD) compared with filtered backprojection (FBP) and conventional IPV.

Materials and methods: Low-contrast and water phantoms were used. Helical scans were conducted with the use of a CT scanner with 64 detectors. The tube voltage was set at 120 kVp; the tube current was adjusted from 60 to 300 mA with a slice thickness of 0.625 mm and from 20 to 150 mA with a slice thickness of 5.0 mm. Images were reconstructed with the FBP, conventional IPV, and IPV-LCD algorithms. The channelized Hotelling observer (CHO) model was applied in conjunction with the use of low-contrast modules in the low-contrast phantom. The noise power spectrum (NPS) and normalized NPS were calculated.

Results: At the same standard and strong levels, the IPV-LCD method improved low-contrast detectability compared with the conventional IPV, regardless of contrast-rod diameters. The mean CHO values at a slice thickness of 0.625 mm were 1.83, 3.28, 4.40, 4.53, and 5.27 for FBP, IPV STD, IPV-LCD STD, IPV STR, and IPV-LCD STR, respectively. The normalized NPS for the IPV-LCD STD and STR images were slightly shifted to the higher frequency compared with that for the FBP image.

Conclusion: IPV-LCD images further improve the low-contrast detectability compared with FBP and conventional IPV images while maintaining similar FBP image appearances.

Keywords

iterative reconstruction, low-contrast detectability, channelized Hotelling observer, multifrequency signal recognition technology, computed tomography

Received 16 March 2022; Accepted 8 June 2022

Introduction

The capacity of diagnostic modalities to detect low-contrast variations in anatomical regions, such as at the borders of white and gray matters, is a critical issue in brain computed tomography (CT) scans. Therefore, a higher radiation dose is required for the detection of low-contrast

¹Department of Medical Radiation Sciences, Faculty of Life Sciences, Kumamoto University, Kumamoto, Japan

²Graduate School of Health Sciences, Kumamoto University, Kumamoto, Japan

³Division of Radiology, Department of Medical Technology, Kyushu University, Fukuoka, Japan

⁴Rad Diagnostic R&D Division, Radiation Diagnostic Systems Division, FUJIFILM Healthcare Corporation, Tokyo, Japan

Corresponding author:

Yoshinori Funama, PhD, Department of Medical Radiation Sciences Faculty of Life Sciences, Kumamoto University, 4-24-1 Kuhonji, Kumamoto 862-0976, Japan.

Email: funama@kumamoto-u.ac.jp



Creative Commons Non Commercial CC BY-NC: This article is distributed under the terms of the Creative Commons Attribution-NonCommercial 4.0 License (<https://creativecommons.org/licenses/by-nc/4.0/>) which permits non-commercial use, reproduction and distribution of the work without further permission provided the original work is attributed as specified on the SAGE and Open Access pages (<https://us.sagepub.com/en-us/nam/open-access-at-sage>).

regions. Iterative reconstruction (IR) is a useful technique used to control the increasing radiation dose while maintaining image quality.¹⁻³ However, researchers reported that despite the improvements in image quality parameters, using model-based IR (MBIR) compared with FBP did not significantly improve low-contrast detectability.⁴ Other researchers also indicated that the texture of images when MBIR is used influenced the radiologist's confidence for image interpretation.⁵ Additionally, IR images with modest radiation dose reduction cannot maintain observer performance.⁶ The reason is attributed to the fact that the noise shifts to lower frequency components, thus resulting in increased image texture roughness.^{7,8} Therefore, IR images with the brain CT need more attention to improve the extremely low image contrast and image texture to maintain observer performance.

Recently, iterative progressive reconstruction with visual modeling (IPV) has been developed to improve low-contrast detectability (IPV-LCD) as a reconstruction method for brain CT. Compared with conventional IPV, the use of IPV-LCD for brain CT employs multifrequency signal recognition technology that improves signal sensitivity by focusing on the low-frequency information for which signal detection of low-contrast objects, such as white and gray matter, is effective. Moreover, the frequency response characteristics of the signal component are modeled with the use of characteristics that are different from those of the noise component. Therefore, the IPV-LCD image expects additional low-contrast detectability improvements compared with filtered backprojection (FBP) and conventional IPV. To investigate a large ensemble of low-contrast detectability, the mathematical model observer with the channelized Hotelling observer (CHO) was applied in our study.⁹⁻¹² The CHO can predict the capacity of human vision to detect low-contrast objects in anatomical images.

The purpose of our study was to focus on low-contrast detectability and to evaluate the performance of IPV-LCD compared with FBP and conventional IPV images in terms of low-contrast detectability at different radiation doses, IR levels, and slice thicknesses using the mathematical model observer.

Materials and methods

Phantom

A low-contrast phantom (CCT189 MITA IQ low-contrast phantom, The Phantom Laboratory Inc., Greenwich, NY, USA) with a diameter of 220 mm was used for low-contrast detectability evaluations in our study.^{13,14} The phantom included eight contrast rods (four each with 10 and 40 mm lengths). At the 10 mm length, the nominal

contrast was 3, 5, 7, and 14 HU with fixed diameters of 15 mm. At the 40 mm length, the combination of nominal contrast and diameter was 3 HU with 10 mm, 5 HU with 7 mm, 7 HU with 5 mm, and 14 HU with 3 mm, respectively. The present study excluded contrast rods at 10 mm length and only used 40 mm length contrast rods mentioned above. Additionally, a water phantom with an outer and inner diameter of $\phi 210$ and $\phi 200$, respectively, was used to evaluate the noise power spectrum.

CT scanning and image reconstruction

A CT scanner with 64 detectors (SCENARIO View, FUJIFILM Healthcare Corporation, Tokyo, Japan) was used in all CT scans. The same area was scanned 50 times with the use of the following scanning parameters: scan mode, helical scan; beam width, 40.0 mm; beam pitch, 0.6; tube voltage, 120 kV; gantry rotation time, 0.5 s; and detector collimation, 64×0.625 mm, with eight different tube currents (i.e., 60, 90, 120, 150, 180, 210, 240, and 300 mA) with a slice thickness of 0.625 mm, and with the use of eight different tube currents (i.e., 20, 30, 40, 50, 60, 90, 120, and 150 mA) with slice thickness of 5.0 mm. The display field-of-view and slice thickness were set at 220 mm and 0.625/5.0 mm, respectively. Filtered backprojection images were reconstructed with a head standard reconstruction kernel (F12). Conventional IPV images were reconstructed at two noise reduction levels [standard 3 (IPV STD), nominal noise reduction: 32%; strong 3 (IPV STR), nominal noise reduction: 56%]. IPV-LCD images were reconstructed at two noise reduction levels [standard 4 (IPV-LCD STD), nominal noise reduction: 32%; strong 3 (IPV-LCD STR), nominal noise reduction: 56%] to obtain the same level of noise reduction.

Low-contrast detectability index

A CHO analysis was used to quantify the low-contrast detectability index.¹⁰ Ten dense-difference of Gaussian (D-DOG) channels were used in the CHO.^{15,16} The channel parameters used were: $\sigma_0 = 0.005$, $\alpha = 1.4$, and $Q = 1.67$, which are the same values proposed in the referred publication.¹⁵ Internal noise was not considered in this study. The inputs were subimage patches that were segmented with the regions-of-interest (ROIs) of signal-present and signal-absent images. The sizes of the ROIs were all 96×96 pixels regardless of the size of the contrast-rod. The ROIs of signal-present images were positioned at the center of gravity of each contrast-rod in images, which were averaged for signal-present slices. The ROIs of signal-absent images were positioned at the same X-Y position of each contrast-rod in the low-contrast rod section. The low-contrast detectability indices were measured by using 800 independent

signal-present and signal-absent image pairs (40 contiguous images \times 20 scans) for a slice thickness of 0.625 mm, and 160 image pairs (eight contiguous images \times 20 scans) for a slice thickness of 5 mm for each combination of contrast-rod, exposure dose (mAs), and reconstruction method. Signal-present and signal-absent images were split into half pairs before training and testing in observer studies.

NPS and normalized NPS

For five reconstruction methods (FBP, IPV STD, IPV STR, IPV-LCD STD, and IPV-LCD STR) with a tube current of 50 mA, 390 images (39 contiguous slice images/scan \times 10 scans) were produced with a slice thicknesses of 0.625 mm. The ROI was defined as the central part of the uniform section image, which consisted of 256×256 pixels. The data were corrected for low-frequency trends using second-order polynomial fitting. The power spectrum of the ROI was obtained by dividing the squared magnitude of the two-dimensional Fourier transform of the noisy ROI image by the area of the ROI. This process was repeated for all 390 images and the mean of the spectra was calculated and defined as the NPS.^{17,18} The normalized NPS was calculated by dividing the NPS value by the area under the NPS curve.

Statistical analysis

The Student's t-test was used to compare the improvement ratio between the conventional IPV and IPV-LCD protocols and between IPV-LCD STD and IPV-LCD STR protocols. A probability (p) value $< .05$ was considered statistically significant. All statistical analyses were performed with the free-source statistical software R (version 4.0.3, The R project for statistical computing, Vienna, Austria, <http://www.rproject.org/>).

Results

Low-contrast detectability index

Figure 1 (slice thickness: 0.625 mm) and Figure 2 (slice thickness: 5.0 mm) show the box plot graphs of the low-contrast detectability index at different contrast-rod diameters between the FBP and each IPV method. At the same standard and strong levels, the IPV-LCD method improved low-contrast detectability compared with conventional IPV, regardless of contrast-rod diameters. The mean CHO values at a slice thickness of 0.625 mm were 1.83, 3.28, 4.40, 4.53, and 5.27 for FBP, IPV STD, IPV-LCD STD, IPV STR, and IPV-LCD STR, respectively (Table 1). The IPV-LCD STD had higher values than conventional IPV's of standard and strong levels (IPV STD and IPV STR). The mean values for a slice thickness of 5.0 mm exhibited similar tendencies as

those for a slice thickness of 0.625 mm. Additionally, the IPV-LCD method obtained higher values than the conventional IPV and FBP methods (Table 1). The areas-under-curves (AUCs) obtained from low-contrast detectability at slice thicknesses of 0.625 mm and 5.0 mm corresponded to 0.62–0.99 and 0.61–1.0 in the case of the FBP, 0.72–1.0 and 0.63–1.0 in the case of IPV-LCD STD, and 0.75–1.0 and 0.63–1.0 with IPV-LCD STR (Figure 3).

Improvement ratio of low-contrast detectability

Figure 4 shows the improvement ratio of the low-contrast detectability of IPV with respect to FBP. At a slice thicknesses of 0.625 mm, the improvement ratios of the low-contrast detectability for IPV/FBP and IPV-LCD/FBP were 1.82 vs 2.43 ($p < .001$) at standard levels, and 2.59 vs 2.91 ($p < .001$) at strong levels, respectively. The improvement ratio of low-contrast detectability increased in the case of IPV-LCD compared with the conventional IPV method, regardless of the IR levels and slice thickness values. Figure 5 shows the improvement ratio of IPV-LCD for conventional IPV on standard and strong levels. The improvement ratios on 0.625 mm and 5.0 mm slice thicknesses were higher in the case of the standard compared with the strong level. Statistically significant differences were observed between IPV-LCD/IPV STD and IPV-LCD/IPV STR at 0.625 mm ($p < .001$) and at 5.0 mm ($p < .01$).

NPS and normalized NPS

Figure 6 presents the NPS and normalized NPS for FBP, conventional IPV, and IPV-LCD. The NPS of IPV-LCD STR images yielded the largest decreases compared with the FBP images over the entire frequency range at a slice thickness of 0.625 mm (Figure 6(a)). The IPV-LCD STD was obtained at the lower NPS curve compared with the IPV STD. The normalized NPS for the IPV-LCD STD and STR images were slightly shifted to the higher frequency compared with that for the FBP image (Figure 6(b)).

Discussion

The study investigated the performance of extremely low image contrast images obtained with IPV-LCD compared with FBP and conventional IPV using the mathematical model observer. In the model observer study, CHO analysis was typically used for the evaluation of the low-contrast detectability because it captures the overall human detectability trends. Compared with conventional IPV, the IPV-LCD method for slice thicknesses of 0.625 mm and 5.0 mm improved the low-contrast detectability values by 34.1% and 16.3% at the standard level and by 29.1% and 14.0% at the strong level, respectively. Additionally, the IPV-LCD at the standard level yielded a more pronounced

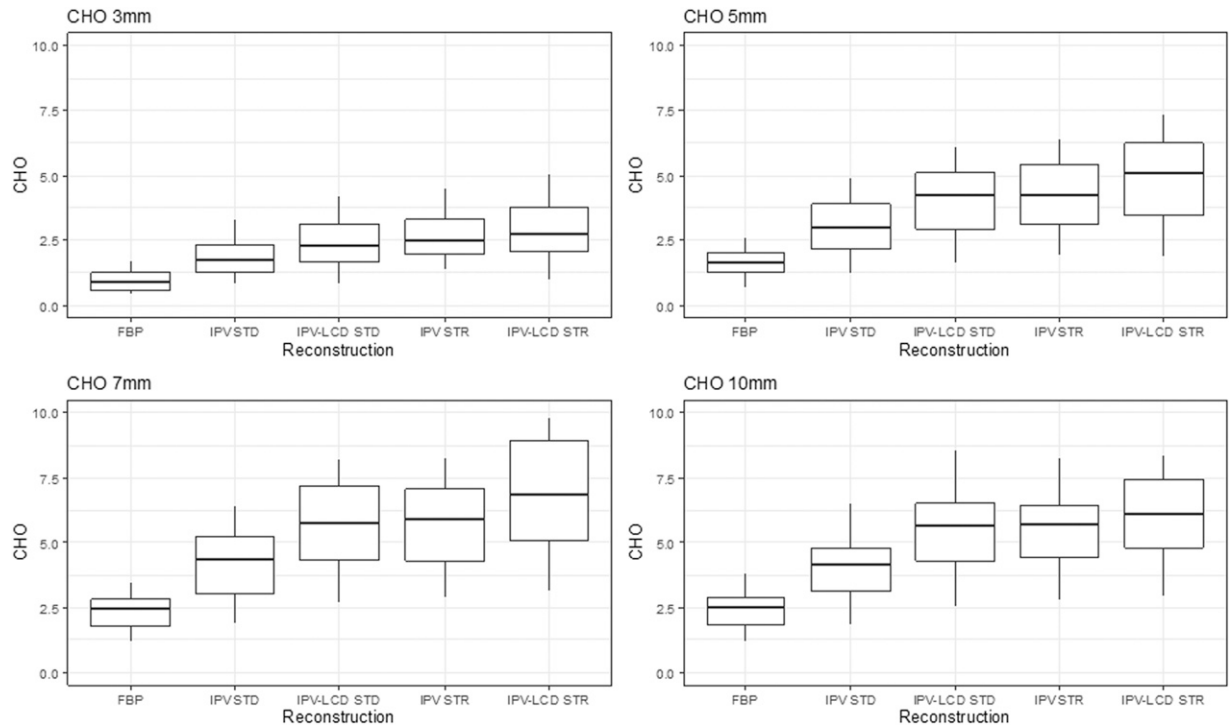


Figure 1. Box plot graphs of the low-contrast detectability index at different contrast-rod diameters between the filtered backprojection (FBP) and each iterative progressive reconstruction with the visual modeling (IPV) method tested herein (slice thickness: 0.625 mm). At the same standard and strong levels, the IPV-low-contrast detectability (LCD) method yielded improved low-contrast detectability compared with the conventional IPV method, regardless of contrast-rod diameters.

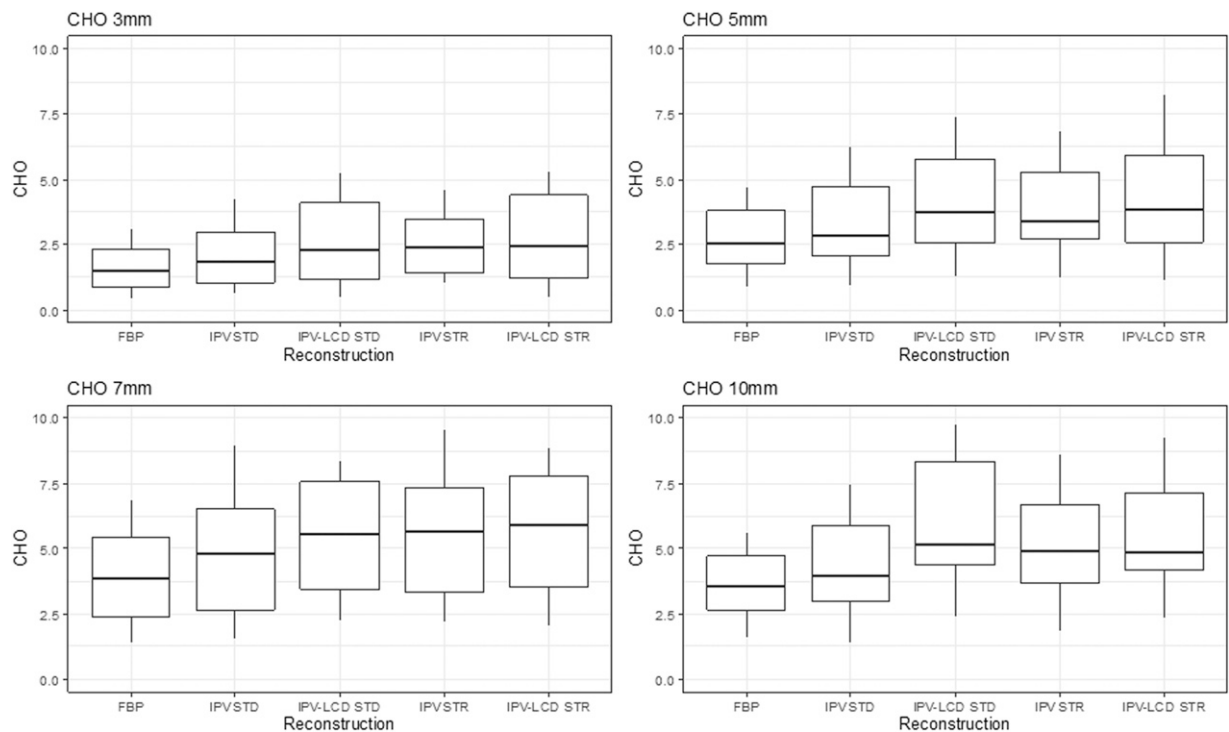


Figure 2. Box plot graphs of the low-contrast detectability index at different contrast-rod diameters between the FBP and each IPV method (slice thickness: 5.0 mm).

Table 1. Mean CHO and standard deviation values with FBP, conventional IPV, and IPV-LCD methods at a slice of 0.625 mm and 5.0 mm.

	Nodule size	FBP	IPV STD	IPV-LCD STD	IPV STR	IPV-LCD STR
0.625 mm	3φ	0.94 ± 0.46	1.85 ± 0.85	2.39 ± 1.12	2.67 ± 1.04	2.89 ± 1.35
	5φ	1.62 ± 0.61	3.01 ± 1.24	4.03 ± 1.54	4.21 ± 1.54	4.86 ± 1.91
	7φ	2.35 ± 0.80	4.21 ± 1.61	5.68 ± 1.98	5.73 ± 1.93	6.84 ± 2.44
	10φ	2.42 ± 0.85	4.06 ± 1.49	5.49 ± 1.93	5.51 ± 1.77	6.51 ± 2.32
	Total	1.83 ± 0.68	3.28 ± 1.30	4.40 ± 1.64	4.53 ± 1.57	5.27 ± 2.01
5.0 mm	3φ	1.62 ± 0.95	2.10 ± 1.28	2.60 ± 1.74	2.56 ± 1.30	2.74 ± 1.81
	5φ	2.71 ± 1.36	3.31 ± 1.82	4.14 ± 2.12	3.87 ± 1.88	4.29 ± 2.37
	7φ	3.95 ± 1.95	4.81 ± 2.56	6.04 ± 2.81	5.52 ± 2.59	6.27 ± 3.06
	10φ	3.72 ± 1.46	4.36 ± 2.09	6.02 ± 2.59	5.17 ± 2.25	6.22 ± 2.93
	Total	3.00 ± 1.43	3.64 ± 1.94	4.70 ± 2.31	4.28 ± 2.00	4.88 ± 2.54

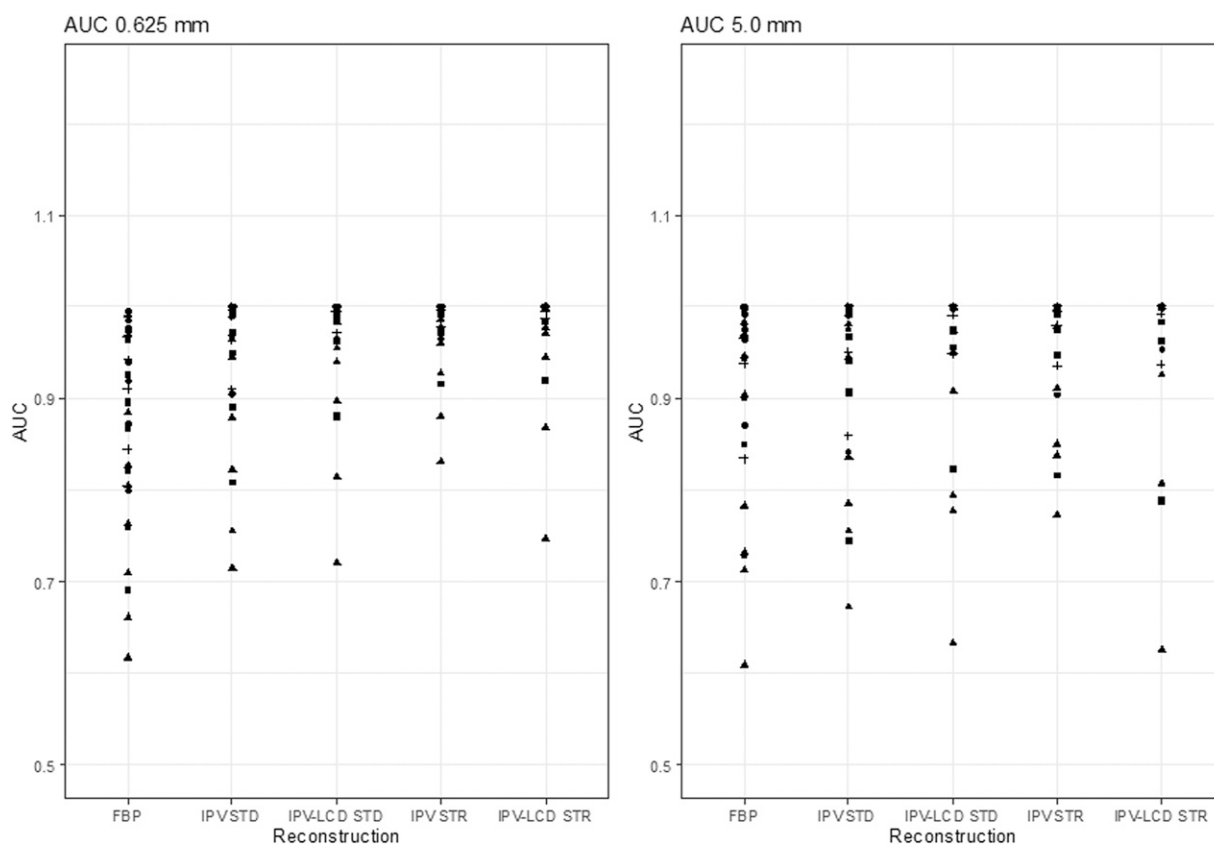


Figure 3. Areas-under-curves obtained from low-contrast detectability at the slice thicknesses of 0.625 mm and 5.0 mm.

improvement ratio than that of the strong level. The NPS with IPV-LCD yielded lower curve values than that with IPV at the same standard or strong levels. The NPS with IPV-LCD and IPV images controlled the lower frequency shift in the reconstruction images so that a similar curve was obtained as that in the case of the FBP images.

IPV-LCD enables additional low-contrast detectability improvements with images with similar appearances as FBP images. The conventional IPV uses the equivalent frequency response between signal and noise components. In

the case of the use of IPV-LCD for brain CT, the frequency response characteristics in the noise frequency component were different from the signal frequency response. The noise in the images included the higher frequency component compared with the frequency of the signal in the image. Moreover, IPV-LCD introduced multifrequency signal recognition technology pertaining to the frequency information of the recognized signal. The technology improved signal sensitivity based on the effective use of the low frequencies responsible for low-contrast signals. For

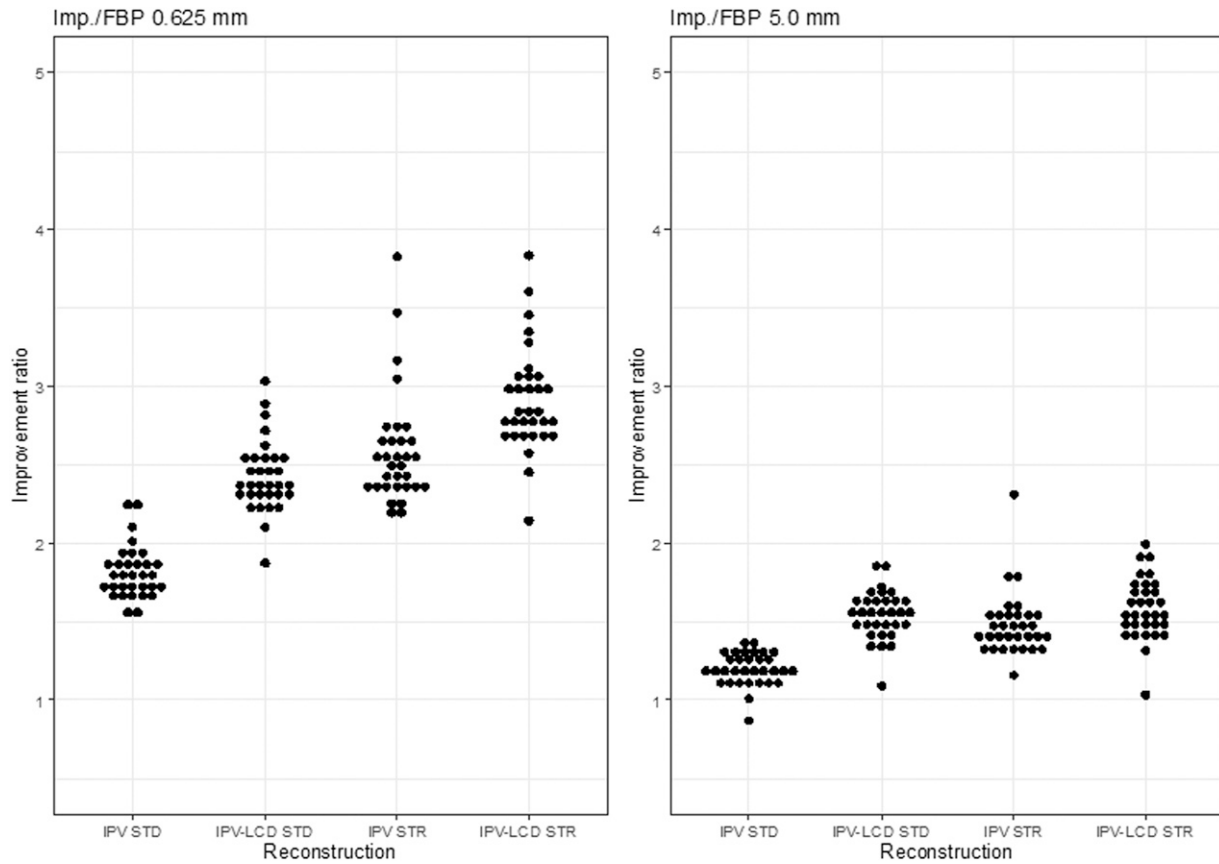


Figure 4. Improvement ratio of the low-contrast detectability of IPV for FBP. The improvement ratio of low-contrast detectability increased in the case of IPV-LCD compared with the conventional IPV method, regardless of the iterative reconstruction levels and slice thickness values.

this reason, the IPV-LCD provided improved visibility of low-contrast signals. Using the technology, the IPV-LCD reduced the image noise and preserved low-contrast signals based on the accurate discrimination of signal and noise frequencies. Therefore, further improvement of low-contrast detectability was achieved with IPV-LCD compared with conventional IPV. The noise characteristics with IPV-LCD are explained by the results of normalized NPS. The peak frequency of the normalized NPS with the IPV-LCD method was shifted slightly to higher frequencies compared with FBP.

Dose optimization is more challenging for low-contrast regions while maintaining image quality, image appearance, and diagnostic confidence. Image quality of conventional IR with the noise reduction in higher IR levels could not be compared with that of FBP owing to the different noise texture patterns, such as “plastic,” and “oil-paint” impressions.⁸ The image appearance influenced the radiologist’s confidence for image interpretation, especially the diagnosis of low-contrast lesions. For instance, in clinical thrombolytic therapy for hyperacute ischemic stroke, accurate localization of early ischemic changes on brain CT is valuable in determining the indication for treatment and prognosis.¹⁹

Therefore, it is necessary to detect the low-contrast area on the affected side, and accurately depict at the same time the parenchymal structure on the healthy side. The improvement of signal sensitivity of low-contrast subjects and the difference in frequency characteristics between signal and noise components by the IPV-LCD can improve lesion detection in left–right comparative reading in brain CT of hyperacute stroke patients. Furthermore, the change in image texture caused by the shifting of noise to the lower frequency side may affect the reliability of image diagnosis during comparative reading with past images. Therefore, the improvement of noise and suppression of image texture changes by the IPV-LCD is anticipated to lead to more accurate diagnosis of hyperacute stroke and scoring outcomes based on the Alberta Stroke Program Early CT Score (ASPECTS).^{19,20}

This study is associated with several limitations. First, our study did not attempt all the combinations of IR levels, but applied two levels, which were associated with equivalent noise reductions between the conventional IPV and IPV-LCD. At these IR levels, standard levels are commonly used in clinical situations. Second, tube current

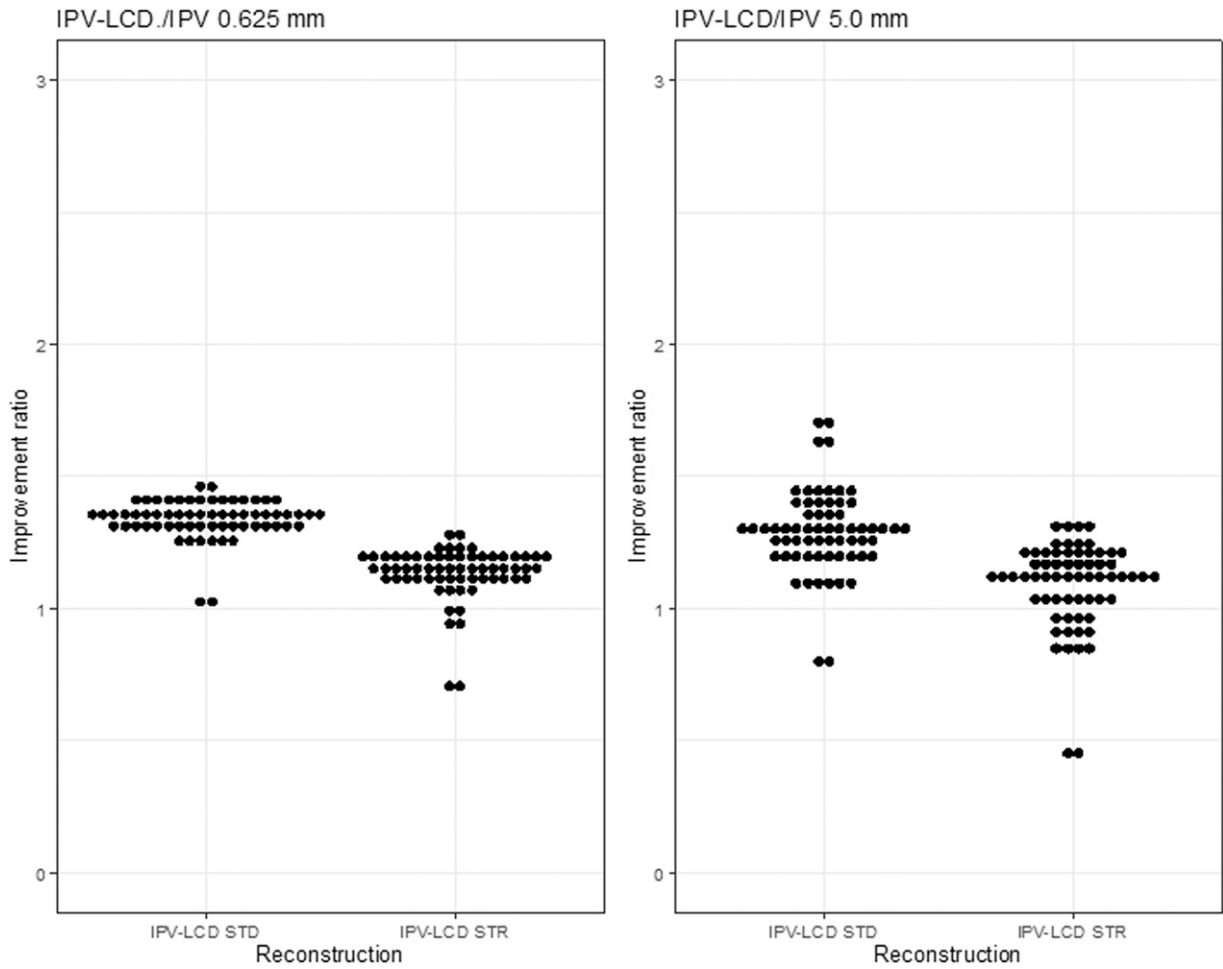


Figure 5. Improvement ratio of IPV-LCD for conventional IPV on standard and strong levels. The improvement ratios were higher at the standard compared with the strong levels.

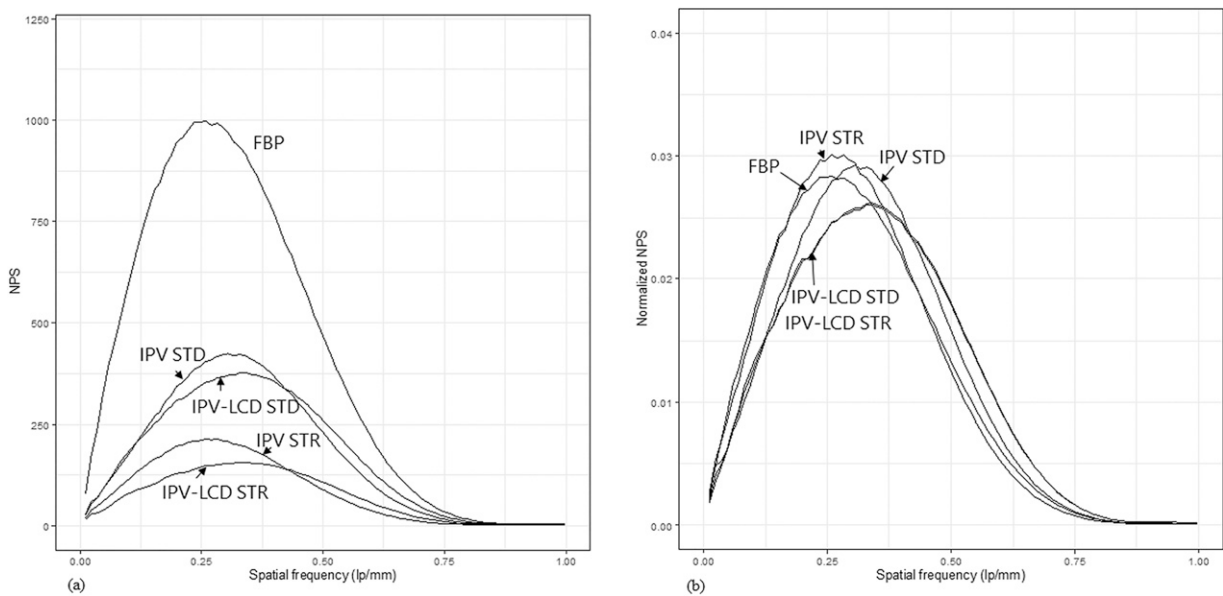


Figure 6. Noise power spectrum (NPS) and normalized NPS for FBP, conventional IPV, and IPV-LCD. The normalized NPS for the IPV-LCD STD and STR images were slightly shifted to higher frequencies compared with the FBP image.

values for slice thicknesses of 0.625 mm and 5.0 mm were predetermined based on the AUC values for low-contrast detectability of FBP images. Finally, the mathematical model observer with the CHO was applied to detect the large ensemble of low-contrast objects. Although the CHO can predict the capacity of human vision, the obtained values may not be exactly the same as those of human observers. Nonetheless, the study results can be directly translated to clinical situations.

In conclusion, our study focuses on low-contrast detectability, and compared IPV-LCD image outcomes with those obtained by FBP and conventional IPV imaging. IPV-LCD images further improve the low-contrast detectability compared with IPV and FBP images while maintaining similar FBP image appearances.

Declaration of conflicting interests

The author(s) declared no potential conflicts of interest with respect to the research, authorship, and/or publication of this article.

Funding

The author(s) disclosed receipt of the following financial support for the research, authorship, and/or publication of this article: This work was supported by the FUJIFILM Healthcare Corporation.

ORCID iD

Yoshinori Funama  <https://orcid.org/0000-0003-1797-9625>

References

1. Love A, Olsson ML, Siemund R, et al. Six iterative reconstruction algorithms in brain CT: a phantom study on image quality at different radiation dose levels. *Br J Radiol* 2013; 86: 20130388.
2. Love A, Siemund R, Hoglund P, et al. Hybrid iterative reconstruction algorithm in brain CT: a radiation dose reduction and image quality assessment study. *Acta Radiol* 2014; 55: 208–217.
3. Southard RN, Bardo DME, Temkit MH, et al. Comparison of iterative model reconstruction versus filtered back-projection in pediatric emergency head CT: dose, image quality, and image-reconstruction times. *AJNR Am J Neuroradiol* 2019; 40: 866–871.
4. Euler A, Stieltjes B, Szucs-Farkas Z, et al. Impact of model-based iterative reconstruction on low-contrast lesion detection and image quality in abdominal CT: a 12-reader-based comparative phantom study with filtered back projection at different tube voltages. *Eur Radiol* 2017; 27: 5252–5259.
5. Laurent G, Villani N, Hossu G, et al. Full model-based iterative reconstruction (MBIR) in abdominal CT increases objective image quality, but decreases subjective acceptance. *Eur Radiol* 2019; 29: 4016–4025.
6. Jensen CT, Wagner-Bartak NA, Vu LN, et al. Detection of colorectal hepatic metastases is superior at standard radiation dose CT versus reduced dose CT. *Radiology* 2019; 290: 400–409.
7. Funama Y, Taguchi K, Utsunomiya D, et al. Image quality assessment of an iterative reconstruction algorithm applied to abdominal CT imaging. *Phys Med* 2014; 30: 527–534.
8. Geyer LL, Schoepf UJ, Meinel FG, et al. State of the art: iterative CT reconstruction techniques. *Radiology* 2015; 276: 339–357.
9. Solomon J, Samei E. Correlation between human detection accuracy and observer model-based image quality metrics in computed tomography. *J Med Imaging (Bellingham)* 2016; 3: 35506.
10. Racine D, Ba AH, Ott JG, et al. Objective assessment of low contrast detectability in computed tomography with channelized hotelling observer. *Phys Med* 2016; 32: 76–83.
11. Ferrero A, Favazza CP, Yu L, et al. Practical implementation of channelized hotelling observers: effect of ROI size. *Proc SPIE Int Soc Opt Eng* 2017; 10132: 101320G.
12. Barrett HH, Abbey CK, Gallas BD, et al. Stabilized estimates of hotelling-observer detection performance in patient-structured noise. *SPIE*, 1998.
13. Khobragade P, Fan J, Rucpich F, et al. Task-based detectability comparison of exponential transformation of free-response operating characteristic (EFROC) curve and channelized hotelling observer (CHO). *SPIE*, 2016.
14. Conzelmann J, Schwarz FB, Hamm B, et al. Development of a method to create uniform phantoms for task-based assessment of CT image quality. *J Appl Clin Med Phys* 2020; 21: 201–208.
15. Abbey CK, Barrett HH. Human- and model-observer performance in ramp-spectrum noise: effects of regularization and object variability. *J Opt Soc Am A Opt Image Sci Vis* 2001; 18: 473–488.
16. Tseng HW, Fan J, Kupinski MA, et al. Assessing image quality and dose reduction of a new x-ray computed tomography iterative reconstruction algorithm using model observers. *Med Phys* 2014; 41: 71910.
17. Boedeker KL, Cooper VN, McNitt-Gray MF. Application of the noise power spectrum in modern diagnostic MDCT: part I. Measurement of noise power spectra and noise equivalent quanta. *Phys Medicine Biology* 2007; 52: 4027–4046.
18. Boedeker KL, McNitt-Gray MF. Application of the noise power spectrum in modern diagnostic MDCT: part II. Noise power spectra and signal to noise. *Phys Medicine Biology* 2007; 52: 4047–4061.
19. Barber PA, Demchuk AM, Zhang J, et al. Validity and reliability of a quantitative computed tomography score in predicting outcome of hyperacute stroke before thrombolytic therapy. ASPECTS study group. *Alberta stroke programme early CT score. Lancet* 2000; 355: 1670–1674.
20. Dzialowski I, Hill MD, Coutts SB, et al. Extent of early ischemic changes on computed tomography (CT) before thrombolysis: prognostic value of the alberta stroke program early CT score in ECASS II. *Stroke* 2006; 37: 973–978.